ACS Catalysis

pubs.acs.org/acscatalysis

Research Article

Electrochemically Engineered, Highly Energy-Efficient Conversion of Ethane to Ethylene and Hydrogen below 550 °C in a Protonic Ceramic Electrochemical Cell

Wei Wu,*[,‖] Lu-Cun Wang,[‖] Hongqiang Hu, Wenjuan Bian, Joshua Y. Gomez, Christopher J. Orme, Hanping Ding, Yanhao Dong, Ting He, Ju Li, and Dong Ding*

Cite This: *ACS Catal.* 2021, 11, 12194–12202

Read Online

ACCESS | Metrics & More | Article Recommendations | Supporting Information

ABSTRACT: Ethylene is one of the largest building blocks in the petrochemical industry, mainly produced by steam cracking of ethane derived from naphtha or shale gas at high temperatures (>800 °C). Despite its technical maturity and economic competitiveness, the thermal steam cracking of ethane is highly energy-intensive. Herein, an electrochemically engineered direct conversion process of ethane to produce hydrogen and ethylene using a planar protonic ceramic membrane reactor with a bi-functional three-dimensional catalytic electrode is reported, with a single-pass ethane conversion of 40% and ethylene yield of 26.7% at 550 °C. Compared with the industrial ethane steam cracking, this method saves process energy input by 45.1% and improves process energy efficiency by 50.6%, based on comprehensive process simulation using Aspen Plus software. Further, steam electrolysis treatment under the solid oxide electrolysis cell mode can regenerate the system's catalytic performance and significantly alleviate catalytic degradation by 74%, demonstrating high techno-economic viability.

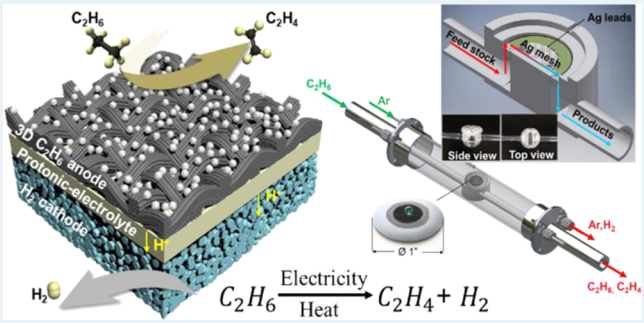

KEYWORDS: *hydrogen production, ethane dehydrogenation, electrochemical synthesis, solid oxide electrochemical cell, bi-functional electrode*

INTRODUCTION

Among the critical building blocks for the petrochemical industry, ethylene is unrivaled in its demand, with production exceeding 143 million tons per year worldwide.[1] The conventional steam cracking process to produce ethylene is the single most energy-consuming process in the chemical industry and is estimated to account for 60% of the production cost and 2/3 of the manufacturing carbon footprint.[2] It is recognized that established ethylene production from steam cracking of ethane or naphtha, optimized throughout the past several decades, is arduous to be replaced without significant breakthroughs in process intensifications and/or catalyst science. Since operating temperature and energy efficiency are the most considered factors in natural gas (NG) upgrading as well as related manufacturing, an ideal alternative ethylene production process through activation of ethane or naphtha should be able to operate at a lower temperature compared with that of the steam cracking (typically 850 °C), with higher energy efficiency.[3]

Solid oxide electrochemical cells (SOCs) that can be used as fuel cells (SOFCs),[4,5] electrolysis cells (SOECs),[6−8] and membrane reactors (SO-EMRs)[9−11] are a promising alternative for more efficient ethylene production.[12] A protonic ceramic electrochemical cell (PCEC), namely, an SOC using a proton-conducting electrolyte, has been used for power-to-chemical/fuel conversions.[13,14] Since it was first reported by Iwahara et al. for steam electrolysis application,[15] a series of perovskite proton-conducting oxides, such as doped $BaCeO_3$[16,17] and $BaZrO_3$,[18] have been applied as electrolyte materials in PCECs. Among them, $BaZr_{0.1}Ce_{0.7}Y_{0.2}O_{3-\delta}$ (BZCY) possesses both high conductivity and good chemical stability.[19] Serra et al. reported direct conversion of methane to aromatics in a BZCY-based membrane tubular reactor with improved aromatic yield and catalyst stability due to the simultaneous extraction of hydrogen and distributed injection of oxide ions.[20] Recently, electrochemical nonoxidative dehydrogenation process (ENDH) of ethane to coproduce ethylene and hydrogen at 400−750 °C, using $BaZr_{0.1}Ce_{0.7}Y_{0.2-x}Yb_xO_{3-\delta}$ (BZCYYb)-based PCEC was re-

Received: July 26, 2021
Published: September 16, 2021

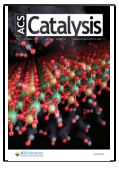

ported.[21−23] The BZCYYb material is the modification of BZCY that exhibits high ionic conductivity and hydrogen permeability at intermediate temperatures,[24] enhancing the ethane nonoxidative dehydrogenation process with merits such as (i) lower operating temperature that results in lower thermal budget and (ii) capability to electrochemically engineer the thermodynamics and kinetics of the desired reaction.[25] In addition, the nonoxidative environment suppresses the competitive reaction between feedstock and product, ensuring high selectivity while alleviating safety considerations and reducing the CO_2 emission. However, the high operating temperature (750 °C) and fabrication complexity of tubular membrane reactors compared with conventional planar membrane reactors decrease its economic attractiveness. Moreover, the conducting behavior of BZCY-based material is temperature sensitive, which exhibits both proton and oxide ion conductivity at elevated temperatures above 700 °C.[26] As a result, the oxidation of C_2H_6 and/or C_2H_4 to CO or CO_2 is highly possible, resulting in low C_2H_4 selectivity. To further explore the proof-of-concept ENDH research, the operating temperature window should be optimized to balance the ethylene yield with electrochemical stability, as well as to develop advanced anode materials that exhibit both anti-coking ability and good electrochemical activity at elevated temperatures.

Here, we present an advanced process named EEDC (electrochemically engineered direct conversion of ethane), to produce hydrogen and ethylene in a planar membrane reactor with controllable product yield, which is not subject to thermodynamic limitation. The catalyst could be adequately regenerated, and the durability is significantly improved after a hydrogen/catalyst cogeneration process under SOEC mode. The key part of the membrane reactor is a PCEC that uses BZCYYb as the electrolyte to enable efficient and accurate control of proton flux during the EEDC process. The full electrochemical cell consists of a thin BZCYYb electrolyte film (~15 μm), a porous Ni-BZCYYb electrode support (~450 μm), and a catalyst-integrated three-dimensional (3D) ultraporous $(PrBa)_{0.95}(Fe_{0.9}Mo_{0.1})_2O_{5+\delta}$ (PBFM) anode (~80 μm). The PBFM material is a nickel-free cation deficient layered perovskite, which has been proven to be an ideal candidate as both anode and cathode application for hydrocarbon fueled SOFC, due to its intrinsic activity for oxygen reduction reaction (ORR), as well as anti-coking ability and catalytic activity for fuel oxidation.[27] In this research, PBFM acts as the anode during the EEDC process while functioning as the steam electrode during the catalyst regeneration process (steam electrolysis in SOEC mode). During the EEDC process, ethane is supplied as feedstock and dehydrogenated to ethylene, electrons, and protons at the 3D PBFM anode. Driven by the external current applied to the cell, the protons conduct through the electrolyte and combine with electrons at the cathode side to form hydrogen (Figure 1a). During the catalyst regeneration process, the atmosphere of the anode side is switched to ambient Ar (10% H_2O in Ar); the PCEC operates in SOEC mode to generate protons and oxygen ions at the PBFM electrode. The generated oxygen ions combine with the carbon deposition in the anode to release CO and/or CO_2, recuperating the catalyst. The PBFM 3D electrode is fabricated by a template-driven high-temperature formation process reported in our previous work.[28−31] The fabrication and characterization details are described in the Material and Methods Section in the Supporting Information (Figure S1, Supporting Information).

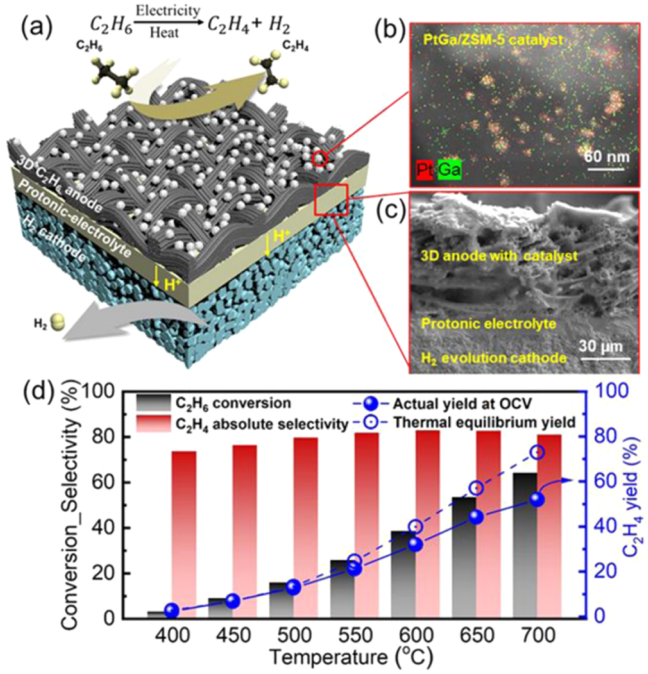

Figure 1. (a) Schematic of the EEDC process of ethane in a proton-conducting electrochemical cell with a 3D fuel electrode. Ethane was fed into the anode and dehydrogenated to ethylene and protons, which was transported through the electrolyte membrane to the cathode and combined with electrons to form hydrogen. (b) Scanning TEM image of the as-prepared PtGa/ZSM-5 catalyst loaded in the 3D anode before testing. (c) Cross-sectional SEM image of the catalyst-integrated electrochemical cell. (d) EEDC performance at different temperatures under OCV conditions. Reaction condition: The anode is swept with a 10/90 mixture of C_2H_6/Ar and the cathode with a 3/3/94 mixture of H_2O/H_2/Ar. 1 atm, feedstock flow rate: 60 mL min^{-1} (47.2 mL cm^{-2} min^{-1}); cathode purging gas flow rate: 120 mL min^{-1} (94.4 mL cm^{-2} min^{-1}).

EXPERIMENTAL SECTION

Fabrication and Integration of the 3D Ceramic Textile Anode. The 3D PBFM electrode was fabricated through a template-driven self-assembly process at 750 °C, followed by integration into the prepared protonic half-cell using a PBFM/BZCYYb suspension (Figure S1a, Supporting Information). The PBFM precursor solution was prepared by dissolving a stoichiometric amount of $Pr(NO_3)_3{\cdot}6H_2O$ (Sigma-Aldrich), $Fe(NO_3)_3{\cdot}9H_2O$ (Sigma-Aldrich), $Ba(NO_3)_2$ (Sigma-Aldrich), and $Mo_7(NH_4)_6O_{24}{\cdot}4H_2O$ (Sigma-Aldrich) in citrate and ethylenediaminetetraacetic acid (EDTA)-NH_3 aqueous solution. Fabric textile (Telio, Montreal, CA) was immersed in that precursor solution overnight, followed by firing at 750 °C for 6 h with a heating rate of 1 °C min^{-1} to form a PBFM ceramic textile. Coupons with a diameter of 1/2 in. were then punched from the sintered ceramic textile. The punched ceramic textile coupon was then bonded on the top of an as-prepared NiO-BZCYYb/BZCYYb half-cell using a 20 wt % PBFM-BZCYYb suspension in ethanol, which contains 12 wt % PBFM powders, 8 wt % BZCYYb powders, and 10 wt % 441-thinner (ElectroScience Laboratories LLC), with a loading of 200 μL cm^{-2}, followed by co-firing at 800 °C for 2 h to form a full cell with a ceramic textile anode. The active anode area is

https://doi.org/10.1021/acscatal.1c03351
ACS Catal. 2021, 11, 12194−12202

1.267 cm^2 (Ø1/2 in.). The NiO-BZCYYb (weight ratio of 60:40)-supported half-cell (~1 in. in diameter) was fabricated by laminating the green tapes prepared by the tape-casting method, following by sintering at 1450 °C in air for 8 h, which is the conventional SOC half-cell fabrication procedure.[30,32] The PBFM/BZCYYb suspension acts not only as the binder between the PBFM textile and the BZCYYb electrolyte but also as the coating material to modify the PBFM textile with sufficient proton conductivity. To measure the anti-coking and chemical stability performance of the PBFM material in EEDC and SOEC conditions, the prepared PBFM textile was exposed to different atmospheres (ambient oxygen and diluted C_2H_6) at 550 °C for 200 h and then followed by characterization using XRD (Figure S1b, Supporting Information). The material under different treating atmospheres presents uniform PBFM patterns without secondary phase peaks, indicating good chemical stability and anti-coking ability in a highly reductive ethane atmosphere. Combined with the SEM and EDS results (Figure S1c, Supporting Information), the template-driven high-temperature self-assembly method is proven to be an effective way to fabricate complicated 3D structures with target stoichiometric composition.

Catalyst Synthesis, Loading, and Characterization. The PtGa/ZSM-5 (CBV 5524 G, Si/Al = 25, surface area 425 $m^2\ g^{-1}$, Zeolyst International) supported catalysts were prepared by the incipient wetness impregnation method.[33] A mixed aqueous solution of tetraammineplatinum nitrate $Pt(NH_3)_4(NO_3)_2$ (Alpha Aesar, 99.9%) and gallium nitrate $Ga(NO_3)_3{\cdot}8H_2O$ (Alpha Aesar, 99.999%) was used for the preparation. The actual loading of Pt and Ga was determined to be 0.175 and 1.02 wt %, respectively, by elemental analysis with the inductively coupled plasma (ICP) optical emission method (ICAP 6500). After impregnation, the catalysts were dried at room temperature in air overnight and further ramped to 120 °C at 1 °C min^{-1} in flowing air and held for 5 h. After drying, the samples were calcined in flowing air by ramping to 600 °C at 1 °C min^{-1} and holding for 2 h. To integrate the catalyst into PCEC, a suspension containing 20 wt % PtGa/ZSM-5, 40 wt % 441-thinner and 40% ethanol was applied on the anode with one-time loading rate of 100 $\mu L\ cm^{-2}$, followed by drying at 80 °C for 1 h. We repeated this procedure to obtain the final catalyst loading of 30 mg (23.7 $mg{\cdot}cm^{-2}$). TGA (STA449F3 NETZSCH Corp.) was used to investigate the carbon deposition of the catalyst-integrated anode. The composite anode was scraped from the tested cells and dried at 80 °C for 30 min in Ar (50 mL min^{-1}). Then, the sample was heated to 780 °C at a rate of 10 °C min^{-1} in air (50 mL min^{-1}). TEM (JEM-2100) was conducted at an accelerating voltage of 300 kV to characterize the morphology of catalysts. A chemical analysis was carried out under TEM using energy-dispersive X-ray spectroscopy (EDS). X-ray photoelectron spectroscopy (XPS) characterization was conducted with a Kratos AXIS Ultra DLD system to determine the surface chemical states and the composition of various catalysts before and after the reaction. The binding energies (BE) were calibrated with reference to the C 1s peak at 284.6 eV.

Reactor Setup and Experiment Parameters. The 1-inch PCEC was sealed in the in-house built reactor (Figure S2, Supporting Information) using glass sealant (Schott, Germany), with the feedstock anode side facing down. Silver mesh and wire were used as the current collector and leads, respectively. After assembly, the reactor was first heated up to 700 °C in ambient air for curing the glass sealant to obtain hermetic and highly insulating seals between ceramic membrane cell and the quartz reacting bed. After a 4 h annealing, the temperature was reduced to 550 °C at 1 °C·min^{-1}. Then, 10% H_2 in Argon (60 mL·min^{-1}) and pure hydrogen (120 mL·min^{-1}) were used to reduce the catalyst in the fuel electrode and NiO in the hydrogen electrode, respectively. After reduction (usually 2 h), 10% H_2 in Ar was replaced by C_2H_6 in the anode side as feedstock, while pure hydrogen in the cathode side was switched to 3% H_2 + 3% H_2O + 94% Ar, as the sweeping gas. The EEDC process started when a fixed current density was applied. The corresponding voltages at different operating temperatures were recorded over time using a Solartron 1400 electrochemical working station. Product composition at the anode side was analyzed using gas chromatography (Shimadzu GC-2010 Plus) at open-circuit voltage as well as at the different current densities to investigate the C_2H_6 conversion and C_2H_4 yield. The product selectivity was calculated on a carbon basis, which was determined by the FID peak area of each major product at the outlet stream. The total flow rate of the outlet gas was measured under each operation condition to account for possible volume changes. C_2H_6 conversion and product selectivity were calculated using the following equations:

$$C_2H_6\ \text{conversion} = \frac{n_{C_2H_{6,\text{inlet}}} - n_{C_2H_{6,\text{outlet}}}}{n_{C_2H_{6,\text{inlet}}}} \times 100\%$$

$$C_2H_4\ \text{selectivity} = \frac{n_{C_2H_4}}{n_{C_2H_{6,\text{inlet}}} - n_{C_2H_{6,\text{outlet}}}} \times 100\%$$

$$CH_4\ \text{selectivity} = \frac{0.5 \times n_{CH_4}}{n_{C_2H_{6,\text{inlet}}} - n_{C_2H_{6,\text{outlet}}}} \times 100\%$$

$$C_{3+}\ \text{selectivity} = 100\% - C_2H_4\ \text{selectivity} - CH_4\ \text{selectivity}$$

Where n is the molar concentration of the species in either the inlet or outlet stream of the reactor.

During the catalyst regeneration process (SOEC mode), the anode inlet gas was first switched to Ar for 30 min to remove C_2H_6 residues. After 10% H_2O in Ar was introduced to the feedstock side, the PCEC was then operated in SOEC mode (80 mA cm^{-2}) to produce hydrogen and regenerate the integrated catalyst at the same temperature as the EEDC process.

Simulation Details. In this study, the EEDC process was simulated using Aspen Plus (version 10) to complete a detailed energy consumption evaluation. The detailed process flow diagram is shown in Figure S3 (Supporting Information), and the assumptions for the simulation are listed in Table S1 (Supporting Information). The EEDC process is designed to have an ethane input of 0.98 million metric ton per year (mtpa) ethylene, which is the same as that from a referenced and medium size steam cracker.[34] The feed ethane diluted with nitrogen is combined with recycled ethane and preheated before feeding into the EEDC reactor, which operates at 550 °C and 15 psi. The EEDC reactor is the core unit of operation in this process. For modeling purposes, the EEDC reactor is represented as three units: (1) a RSTOIC reactor (ELECRTOR) for the EEDC reactor; (2) a separator to separate the anode products (ethylene), the cathode product (H_2), and solid carbon "coke" (RECSEP); and (3) a regeneration unit for

https://doi.org/10.1021/acscatal.1c03351
ACS Catal. 2021, 11, 12194−12202

decoking inside the EEDC reactor. These three separate units in the model represent a single EEDC reactor, while the latter two units do not exist in an actual plant. Similar to thermal steam cracking, the process chemistry of the EEDC reactor was explained by a complex set of reactions that are based on a free radical mechanism.[34,35] Out of these reactions, six possible reactions that adequately define the net effect of the chemistry were considered in this study (Table S2, Supporting Information). The fractional conversion for each reaction in the EEDC was optimized to assure that the obtained simulated product yields agree with the experimental results. The simulated results for ethylene, ethane, and C_{3+} heavy hydrocarbons match well with laboratory results with a variance of less than 0.05%. The single-pass ethylene yield in laboratory results varied with the operating temperature and the applied current. At 550 °C, the single-pass ethylene yield at the anode side was measured as 25.7 wt % at the applied current of 40 mA cm^{-2}. The product stream from the EEDC reactor was then compressed with inter-stage cooling to reach 10 °C with 150 psi. Then, a refrigeration system was applied to further reduce the temperature for downstream cryogenic separation in liquid condition at the specified temperature (−150 °C) and pressure (145 psi). In this system, a three-step cascade process was modeled separately using phase separators, throttle valves (i.e., Joule−Thomson valves), and coil-wound heat exchangers, referred to as ColdBox in Aspen Plus simulation. The separation section consists of conventional cryogenic distillation separation and membrane separation. Considering the recent development of membrane separation for some gas separations and the high energy requirements of cryogenic distillation, membrane separation systems are employed to separate hydrogen, methane, and nitrogen to reduce the overall energy consumption. Other hydrocarbon separations are conducted via cryogenic distillation columns, which include five columns. On the other hand, a steam cracking process is commonly grouped into three sections: reaction (pyrolysis), compression, and separation. The reaction (pyrolysis) section comprises a cracker, which is the heart of the ethylene process plant and has the maximum energy consumption due to the high endothermicity of the reactions occurring in the cracker. Cracking products are compressed in stages to the desired pressure to effectively separate the produced ethylene as a product from other compounds in cryogenic separation trains. The process chemistry for steam cracking of ethane is as follows: a single-pass conversion of C_2H_6 is 60%; the yields of all products after the cracker by mass % are C_2H_6 − 40% (unreacted), C_2H_4 − 52.4%, H_2 − 3.8%, CH_4 − 2.6%, etc. These yields are based on pure hydrocarbons; steam is excluded.[34] The process model provides an overall mass and energy balance. The two processes are compared (Table S3, Supporting Information): EEDC and steam cracker. It is worth noting that the off-gases generated from the steam cracking process, including hydrogen, methane, acetylene, propylene, propane, and butadiene, were used in the form of equivalent of natural gas for heating and were balanced in the final energy of the fuel required. Consequently, there is no by-product shown for steam cracking, whereas hydrogen and other gases are listed as by-products for the EEDC process. The produced H_2 from the regeneration process (SOEC mode) was also included in the energy efficiency calculation, although its influence is negligible due to the limited regeneration time. Thus, the overall process energy efficiency of EEDC is calculated as 75%, higher than 47% of steam cracking, even though this process has higher energy consumption for one metric ton of ethylene produced, 100 MMTBU vs 90 MMBTU for steam cracking.

The energy consumption for the thermal steam cracking of ethane was obtained from literature data.[34] The energy consumption of EEDC process is calculated from Aspen Plus simulation (Table S4, Supporting Information). The energy input includes electricity, nonelectricity (mainly thermal), and feed ethane. The energy output are energy contents of all generated products. The results were used to evaluate the energy efficiency of the process. Energy efficiency was calculated by the following equation:

$$\text{efficiency}(\%) = \frac{\sum(\text{energy of all products})}{\sum(\text{energy of all inputs})} = \frac{\sum(\text{flow rate} \times \text{high heat value})}{\text{energy of ethane feedstock} + \sum(\text{energy consumption})}$$

RESULTS AND DISCUSSION

The novel PtGa/ZSM-5 catalysts (Figure 1b) were prepared by the incipient wetness impregnation method and integrated into the 3D PBFM anode before the test with a solid loading of 23.7 mg·cm^{-2} (30 mg total), as shown in Figure 1c. Scanning transmission electron microscopy-energy-dispersive X-ray spectroscopy (STEM-EDS) mapping showed that the Pt and Ga components are homogeneously mixed and well dispersed on the support surface in the form of clusters and nanoparticles with sizes ranging from 2 to 30 nm (Figure 1b). The EEDC incorporates superb thermal catalytic performance of the PtGa/ZSM-5 catalyst, which was typically represented by the C_2H_6 conversion and C_2H_4 yield at open-circuit voltage (OCV) conditions (Figure 1d). The external current-free membrane reactor at OCV conditions acts as a fixed bed reactor, and the catalytic performance simply comes from thermal cracking. As shown in Figure 1d, both ethane conversion and ethylene yield increase with temperature, while the ethylene selectivity reaches a peak value of 82% at 600 °C. The decrease in selectivity above 600 °C may result from side reactions like coking and ethylene coupling (Figure S4, Supporting Information). The experimental ethylene yield (solid blue curve) reached the thermal equilibrium value (dashed blue curve) below 550 °C, indicating the PtGa/ZSM-5 is a highly efficient catalyst for nonoxidative dehydrogenation of ethane (NDH) to ethylene at reduced temperatures, especially below 550 °C.

The EEDC process is conducted in an in-house built dual-zone reactor with a quartz reacting bed inside to hold 1-inch button PCEC (Figure S2, Supporting Information). To balance the catalytic performance (i.e., ethylene yield) with the PCEC electrochemical performance in both EEDC and SOEC mode, an optimized operating temperature window is required. Increasing the EEDC operating temperature results in a higher ethylene yield (Figures 1d and S5a, Supporting Information) and leads to greater practical potential. Moreover, the PCEC demonstrates lower overpotential in EEDC mode and higher steam electrolysis performance at a fixed electrolysis voltage under SOEC mode, as shown in Figure S6 (Supporting Information). However, when the temperature is lower than 450 °C, both electrolyte conductivity and electrode catalytic performance drop dramatically and result in the deterioration of ohmic and polarization losses. The EEDC

https://doi.org/10.1021/acscatal.1c03351
ACS Catal. 2021, 11, 12194−12202

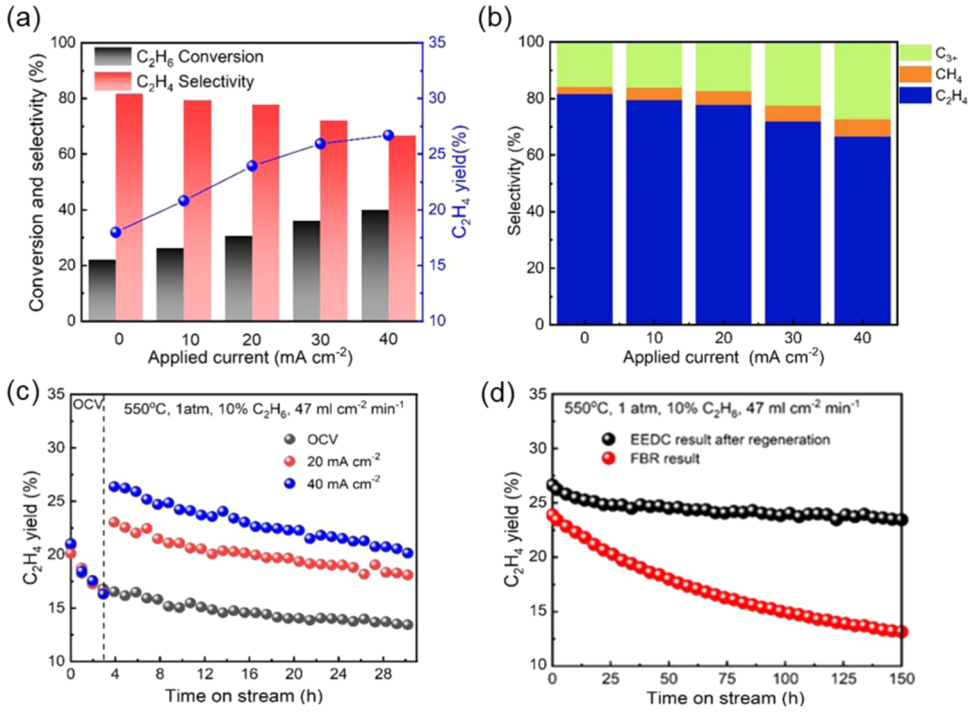

Figure 2. Electrocatalytic performance of the EEDC process. (a) C_2H_6 conversion and C_2H_4 yield as a function of applied current at 550 °C. (b) Product selectivity under different applied current densities. (c) C_2H_4 yields versus time at different applied current densities. (d) Improved EEDC catalytic durability at 40 mA·cm^{-2} after regeneration for four times under SOEC mode.

energy input related to the reactor overpotential thus increases and reduces the techonomic benefits. According to the catalytic performance at OCV conditions, there is a trade-off between EEDC operation temperature (represented by energy consumption) and EEDC efficiency (represented by ethylene selectivity and yield). On the one hand, operation at temperatures below 450 °C would significantly lower the catalytic performance in terms of ethane conversion and ethylene yield, as well as the electrochemical performances in terms of proton conductivity. On the other hand, when the operating temperature was raised above 600 °C, the Faraday efficiency started to drop substantially with temperature, as shown by the Faraday efficiency measurement results (see Figure S7). In addition, we have detected CO_2 in the product stream, resulting from ethane oxidation, when the temperature reached 700 °C. Note that we have not detected any CO_2 in the product stream at 550 °C and below, since the BZCYYb material demonstrates almost pure proton-conducting behavior at lower temperatures (<600 °C). This observation strongly suggests that oxidative dehydrogenation may occur at higher temperatures with oxygen-containing species on the cathode side, which coincides with the fact that BZY-based proton conductors started to exhibit oxide ion (O^{2-}) conductivity at this temperature.[20,36] Since CO_2 poisoning of BZCYYb electrolyte material is a critical concern in electrochemical processing of hydrocarbons, one of the unique aspects of this work lies in the strict nonoxidative atmosphere, i.e., no oxygen-containing species at the anode side during EEDC operation, which eliminates the possibility of CO/CO_2 formation. Moreover, from an energy and economic point of view, operations at temperatures higher than 600 °C would dramatically increase the thermal budget and therefore decrease the attractiveness of the EEDC process compared with the conventional steam cracking process. Therefore, we suggest that in EEDC application, an ideal operating temperature window for the EEDC process would be between 450 to 600 °C, at which the catalyst has reasonable performance while the PCEC maintains sufficient electrochemical activity and Faraday efficiency.

To explore the EEDC process more practically, we focus on the ethane concentration of 10%, and operate under different current inputs at 550 °C, at which the BZCYYb material maintains close to unit proton conductivity,[19] but the C_2H_4 yield increases by 10 times of that at 400 °C (Figure S5b, Supporting Information). At 550 °C, both ethane conversion and ethylene yield increase with the applied current, as shown in Figure 2a. The ethylene yield increases from 17.9 to 26.7% when the applied current increases from 0 to 40 mA cm^{-2}, while the ethylene absolute selectivity decreases from 81.7 to 66.7%. The ethylene yield started to level off when the applied current is higher than 30 mA cm^{-2}, due to the increased selectivity of higher (C_{3+}) hydrocarbons (Figure 2b) resulting from side reactions, including coupling and metathesis of the produced ethylene and its derivatives (Figure S8, Supporting Information).

We also evaluated the performance of the solid oxide cell for ethane conversion in the absence of the PtGa/ZSM-5 catalyst. The results showed that without the catalyst, the ethane conversion was only about 7.5% at 600 °C under OCV conditions, and it slightly increased to less than 9% even with an applied current of up to 40 mA·cm^{-2}, which is significantly lower than the results (close to 40%, see Figure 1d) obtained with the catalyst incorporated. Clearly, the integration of highly active ethane dehydrogenation catalyst to the cell is necessary to achieve high ethane conversion at relatively lower temperatures (<600 °C). The enhanced ethane conversion by the applied current may result from the increased hydrogen separation from the product stream, which shifts the reaction

https://doi.org/10.1021/acscatal.1c03351
ACS Catal. 2021, 11, 12194−12202

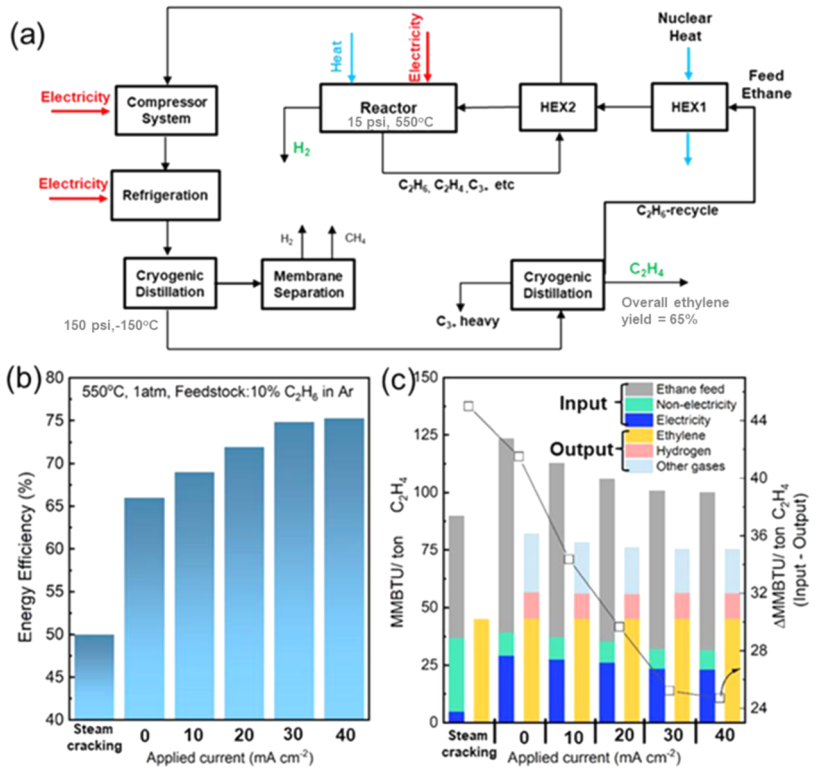

Figure 3. Process simulation results based on EEDC technology. (a) Simplified process flow diagram for ethane to ethylene via EEDC. (b) Energy efficiency of the EEDC system at different applied currents. (c) Specific input energy consumption, output energy production, and net energy requirement for one-ton ethylene produced at different applied current densities.

equilibrium. Nevertheless, the potential contribution of electrochemically driven ethane conversion could not be ruled out.

Figure 2b shows the ethylene, methane, and C_{3+} product selectivity variation at different applied currents. The applied current has negative effects on the ethylene selectivity but positive effects on CH_4 and C_{3+} product selectivity. The positive effect of electrical current on C_{3+} formation may be associated with H_2 removal, which shifts the thermodynamic equilibrium to favor the formation of higher hydrocarbons. The faster H_2 removal from the product stream at higher electrical current would lead to an increase in local coverage/concentration of ethylene intermediates, which in turn will increase the rate of coupling and metathesis reactions among the ethylene product and its derivatives, especially alkenes, thus increased C_{3+} formation. Since CH_4 is formed via the cleavage of C−C bond in ethane molecule, the increased CH_4 formation may originate from activated C−C bond breaking of ethane at higher electrical current. Product selectivity has obvious dependence on the external current applied. Figure 2c shows the ethylene yield versus time at different applied currents. The deteriorated catalyst stability at higher applied current mainly originates from increased coking within the anode (Figure S9a,b, Supporting Information), which may result from the deep dehydrogenation of ethylene at higher conversion on Pt-active sites.[37] However, the catalytic performance can be regenerated, and the durability was even improved after a catalyst regenerative treatment, as shown in Figure 2d. During the catalyst regeneration process, the PCEC was operated under SOEC mode to conduct steam electrolysis ($H_2O \rightarrow H_2 + O_2$) as well as to remove the coke ($C + O_2 \rightarrow CO$ or CO_2). It should be noted that during the regeneration process, water itself may also directly react with coke at the operating temperature via the reaction: $C + H_2O \rightarrow CO + H_2$. The SOEC operation broke in every 30-h of EEDC test, (Figure S10a, Supporting Information). The degradation rate drops from 0.85% h^{-1} (first run) to 0.22% h^{-1} (the fifth run), mainly due to the suppression of coke formation (Figure S9c,d, Supporting Information). The SOEC treatments improved both initial C_2H_4 yield and system durability (Figure S10, Supporting Information), which is believed to result from both macroscopic catalyst redistribution from 3D anode reconstruction under SOEC mode (Figure S11, Supporting Information) and the microscopic PtGa particles redistribution on the ZSM-5 surface (Figure S12, Supporting Information). XPS characterization of the catalyst before and after the reaction suggested that both Pt and Ga species were reduced to a metallic state and existed in the form of PtGa alloy under reaction conditions (Figure S13 and Table S5). The increased C 1s peak intensity on the used catalyst (Figure S13c) also indicated the deposition of C species on the surface during the reaction, which is consistent with the TGA results (Figure S9). During SOEC operation, the anode hollow fibers bridged each other and lowered both ohmic and polarization resistance by forming additional physical connections for charge transfer, which has also been observed in our previous work on steam electrolysis.[30] The integrated catalysts were accordingly redistributed in the 3D anode and resulted in an increase in the catalyst utilization indicated by the increase of the initial C_2H_4 yield of each cycle (Figure S10b, Supporting Information). The redistribution of Pt and Ga on the ZSM-5 surface makes the active sites more uniform and produces more accessible Pt sites, resulting in improved catalytic durability. The durability enhancement phenomenon was

https://doi.org/10.1021/acscatal.1c03351
ACS Catal. 2021, 11, 12194−12202

also observed during the catalyst regeneration for ethane dehydrogenation at 450−650 °C.[38] Overall, both the performance evaluation and structure characterization results suggest that the coking-induced catalyst deactivation should dominate the degradation mechanism of the EEDC system since no obvious signs of cell degradation have been observed after long-term operations.

To evaluate the practical implications of this novel EEDC process, technical feasibility and energy efficiency were preliminarily analyzed by performing a comprehensive process simulation using Aspen Plus software. In addition, the results were compared with those of steam cracking, which is the predominant manufacturing method for ethylene production in the United States. Considering EEDC is still at its early research stage, its single-pass ethylene yield is still limited and varied with operating temperature and applied current. At 550 °C, the ethylene yield ranged from 17.9 to 26.7% for the applied current from 0 to 40 mA cm^{-2} (Figure 2a for yield). With recycling and system integration, the overall ethylene yield was projected to be 65% at 40 mA cm^{-2} (Table S3, Supporting Information). On the other hand, the single-pass ethylene yield for steam cracking is 52.4%. Therefore, these two processes were designed to have similar annual ethane feed flow rate, 0.98 million ton/year. Figure 3a demonstrates a simplified schematic process flow diagram (PFD) for EEDC process, while the detailed PFD obtained from Aspen Plus simulation is shown in Figure S3 (Supporting Information). The process mainly consists of four process sections: reaction, compression and cooling, refrigeration, and separation, among which the PCEC reactor is the core unit of operation.

Heat recuperation was integrated to increase the overall energy efficiency. Both feed ethane and recycled ethane streams were preheated using an external heat source and the ethylene product stream before entering the PCEC reactor. The ethylene product stream was also used for boiler heat required for cryogenic distillation columns. Furthermore, hydrogen generated from the EEDC process provides significant energy credit. According to the simulation, the overall energy efficiency of EEDC ranges from 66 to 75.3% for different applied currents, achieving up to 50.6% improvement in energy efficiency when compared to the 50% in steam cracking,[34] as shown in Figure 3b. In terms of specific energy consumption for one-ton ethylene produced, about 100 MMBTU is required for EEDC process at 40 mA cm^{-2} (Figure 3c), compared to 90 MMBTU for the ethane steam cracking process, among which feedstock ethane is the major energy requirement, while the steam cracking requires almost 3 times nonelectricity energy higher than EEDC. For energy outputs, the EEDC generates up to 20 MMBTU more energy than steam cracking. We calculated the net energy requirement (ΔMMBTU, $E_{input} - E_{output}$) for EEDC and steam cracking processes. Compared to steam cracking, the net energy requirement reduced from 45 to 24.7 MMBTU, presenting a 45.1% reduction in energy requirement (Figure 3c). The superiority of this EEDC process compared with the conventional thermal cracking process mainly lies in two factors: the unique advantages of PCECs in product separation, which simplifies the production process and the plant layout; and the produced hydrogen as energy credit. However, the ethylene single-pass yield in EEDC is half of the mature steam cracking technology, resulting in the ethane feed energy to be still the dominant part for overall energy consumption in EEDC, requiring 68−84 MMBTU/ton of produced ethylene at different applied currents, accounting for about 68% of the overall processing energy. Considering the early research stage of current EEDC technology, it holds more superiority than steam cracking if its ethylene yield could be enhanced in the future through the improvement of electrocatalysts and cell component materials.

CONCLUSIONS

We demonstrated efficient direct conversion of ethane to hydrogen and ethylene using a protonic ceramic electrochemical system below 550 °C, not subject to the thermal equilibrium ethane conversion limitation. This work highlights the innovation of PtGa-ZSM-5 catalyst along with a catalyst-integrated protonic electrochemical cell system with novel PBFM ceramic textile anodes, enabling high-efficient ethylene production and system durability. Further, we performed a comprehensive process simulation using Aspen Plus software to evaluate the practical implications of this technology and compare it with the industrial ethane thermal cracking. Our method represents a breakthrough in the development of energy processing intensification processes and shows great potential for distributed applications that can be operated on an on-demand basis, which will benefit facile integration with low-carbon heat and renewable electricity for an integrated/hybrid energy system.

ASSOCIATED CONTENT

Supporting Information

The Supporting Information is available free of charge at https://pubs.acs.org/doi/10.1021/acscatal.1c03351.

Fabrication procedures of electrochemical cell with 3D anode; XRD patterns and EDS mapping of PBFM material under different atmospheres; schematic of the in-house built dual-zone reactor; detailed process flow diagram of an EEDC process for Aspen Plus simulation; selectivity of various hydrocarbon products in the EEDC process at different temperatures above 600 °C under OCV conditions; C_2H_6 conversion and C_2H_4 yield at different applied currents, operating temperatures, and C_2H_6 feedstock concentration; electrochemical performance under EEDC and SOEC modes; results of Faraday efficiency measurement; GC raw data showing the formation of higher (C_{3+}) hydrocarbon products in the EEDC process; TGA results and calculated coke content under different applied currents and after regeneration; C_2H_4 yield during each operation cycle with intermittent regeneration; cell resistance and SEM images of the integrated anode before and after the test; STEM image of PtGa/ZSM-5 catalyst before and after EEDC process; XPS result of the PtGa/ZSM-5 catalyst before and after reaction; assumptions for the Aspen Plus simulation of the EEDC process; reactions and corresponding conversions inside the EEDC reactor at 40 mA·cm^{-2} assumed for Aspen Plus simulation; process result summary of ethylene production from steam-ethane cracking and EEDC at an applied current density of 40 mA cm^{-2}; specific energy input and output for the EEDC process; surface chemical composition of the PtGa/ZSM-5 catalyst before and after reaction (PDF)

https://doi.org/10.1021/acscatal.1c03351
ACS Catal. 2021, 11, 12194−12202

AUTHOR INFORMATION

Corresponding Authors

Wei Wu − *Department of Energy & Environmental Science and Technology, Idaho National Laboratory, Idaho Falls, Idaho 83415, United States*; Email: wei.wu@inl.gov

Dong Ding − *Department of Energy & Environmental Science and Technology, Idaho National Laboratory, Idaho Falls, Idaho 83415, United States*; orcid.org/0000-0002-6921-4504; Email: dong.ding@inl.gov

Authors

Lu-Cun Wang − *Department of Energy & Environmental Science and Technology, Idaho National Laboratory, Idaho Falls, Idaho 83415, United States*

Hongqiang Hu − *Department of Energy & Environmental Science and Technology, Idaho National Laboratory, Idaho Falls, Idaho 83415, United States*

Wenjuan Bian − *Department of Energy & Environmental Science and Technology, Idaho National Laboratory, Idaho Falls, Idaho 83415, United States; Department of Chemical & Materials Engineering, New Mexico State University, Las Cruces, New Mexico 88003, United States*

Joshua Y. Gomez − *Department of Energy & Environmental Science and Technology, Idaho National Laboratory, Idaho Falls, Idaho 83415, United States; Department of Chemical & Materials Engineering, New Mexico State University, Las Cruces, New Mexico 88003, United States*

Christopher J. Orme − *Department of Energy & Environmental Science and Technology, Idaho National Laboratory, Idaho Falls, Idaho 83415, United States*

Hanping Ding − *Department of Energy & Environmental Science and Technology, Idaho National Laboratory, Idaho Falls, Idaho 83415, United States*

Yanhao Dong − *Department of Nuclear Science and Engineering, Massachusetts Institute of Technology, Cambridge, Massachusetts 02139, United States*

Ting He − *Department of Energy & Environmental Science and Technology, Idaho National Laboratory, Idaho Falls, Idaho 83415, United States*

Ju Li − *Department of Nuclear Science and Engineering, Massachusetts Institute of Technology, Cambridge, Massachusetts 02139, United States*; orcid.org/0000-0002-7841-8058

Complete contact information is available at: https://pubs.acs.org/10.1021/acscatal.1c03351

Author Contributions

[‖]W.W. and L.-C.W. contributed equally to this work.

Author Contributions

D.D. conceived, designed, and supervised the project. W.W. and L.W. developed the catalyst, fabricated the reactor and cells, conducted electrochemical tests, and analyzed the data. H.H. did the process simulations. J.G. conducted the reactor design and test. H.D. helped with the reactor design and data analysis. C. O. performed the TGA test. W.B. helped with the cell fabrication and electrochemical tests. Y.D. performed the STEM test. T.H. and J.L. helped with catalyst design and data analysis. W.W., L.W., and H. H. wrote the manuscript.

Notes

The authors declare no competing financial interest.

ACKNOWLEDGMENTS

This work was supported by the U.S. Department of Energy (USDOE), Office of Energy Efficiency and Renewable Energy (EERE), Advanced Manufacturing Office (AMO) R&D Projects Emerging Research Exploration under DOE Idaho Operations Office under Contract No. DE-AC07-05ID14517.

REFERENCES

(1) Fabiano, B.; Pistritto, F.; Reverberi, A.; Palazzi, E. Ethylene−air mixtures under flowing conditions: a model-based approach to explosion conditions. *Clean Technol. Environ. Policy* **2015**, *17*, 1261−1270.

(2) Ren, T.; Patel, M.; Blok, K. Olefins from conventional and heavy feedstocks: Energy use in steam cracking and alternative processes. *Energy* **2006**, *31*, 425−451.

(3) Gao, Y.; Neal, L. M.; Ding, D.; Wu, W.; Baroi, C.; Gaffney, A.; Li, F. Recent Advances in Intensified Ethylene Production−A Review. *ACS Catal.* **2019**, *9*, 8592−8621.

(4) Hibino, T.; Hashimoto, A.; Inoue, T.; Tokuno, J.-i.; Yoshida, S.-i.; Sano, M. A low-operating-temperature solid oxide fuel cell in hydrocarbon-air mixtures. *Science* **2000**, *288*, 2031−2033.

(5) Wachsman, E. D.; Lee, K. T. Lowering the temperature of solid oxide fuel cells. *Science* **2011**, *334*, 935−939.

(6) Ebbesen, S. D.; Jensen, S. H.; Hauch, A.; Mogensen, M. B. High temperature electrolysis in alkaline cells, solid proton conducting cells, and solid oxide cells. *Chem. Rev.* **2014**, *114*, 10697−10734.

(7) Ali, S.; Sørensen, K.; Nielsen, M. P. Modeling a novel combined solid oxide electrolysis cell (SOEC)-Biomass gasification renewable methanol production system. *Renewable Energy* **2020**, *154*, 1025−1034.

(8) Fu, Q.; Mabilat, C.; Zahid, M.; Brisse, A.; Gautier, L. Syngas production via high-temperature steam/CO_2 co-electrolysis: an economic assessment. *Energy Environ. Sci.* **2010**, *3*, 1382−1397.

(9) Malerød-Fjeld, H.; Clark, D.; Yuste-Tirados, I.; Zanon, R.; Catalan-Martinez, D.; Beeaff, D.; Morejudo, S. H.; Vestre, P. K.; Norby, T.; Haugsrud, R.; Serra, J. M.; Kjolseth, C. Thermo-electrochemical production of compressed hydrogen from methane with near-zero energy loss. *Nat. Energy* **2017**, *2*, 923−931.

(10) Sun, S.; Huang, K. Efficient and selective ethane-to-ethylene conversion assisted by a mixed proton and electron conducting membrane. *J. Membr. Sci.* **2020**, *599*, No. 117840.

(11) Chen, L.; Chen, F.; Xia, C. Direct synthesis of methane from CO_2−H_2O co-electrolysis in tubular solid oxide electrolysis cells. *Energy Environ. Sci.* **2014**, *7*, 4018−4022.

(12) Wu, W.; Hu, H.; Ding, D. Low-temperature ethylene production for indirect electrification in chemical production. *Cell Rep. Phys. Sci.* **2021**, No. 100405.

(13) Li, M.; Hua, B.; Wang, L.-C.; Sugar, J. D.; Wu, W.; Ding, Y.; Li, J.; Ding, D. Switching of metal−oxygen hybridization for selective CO_2 electrohydrogenation under mild temperature and pressure. *Nat. Catal.* **2021**, *4*, 274−283.

(14) Serra, J. M. Electrifying chemistry with protonic cells. *Nat. Energy* **2019**, *4*, 178−179.

(15) Iwahara, H.; Uchida, H.; Ono, K.; Ogaki, K. Proton conduction in sintered oxides based on $BaCeO_3$. *J. Electrochem. Soc.* **1988**, *135*, 529−533.

(16) Lyagaeva, J.; Danilov, N.; Vdovin, G.; Bu, J. F.; Medvedev, D.; Demin, A.; Tsiakaras, P. A new Dy-doped $BaCeO_3$-$BaZrO_3$ proton-conducting material as a promising electrolyte for reversible solid oxide fuel cells. *J. Mater. Chem. A* **2016**, *4*, 15390−15399.

(17) Iwahara, H.; Uchida, H.; Morimoto, K. High-temperature solid electrolyte fuel-cells using perovskite-type oxide based on $BaCeO_3$. *J. Electrochem. Soc.* **1990**, *137*, 462−465.

(18) Shafi, S. P.; Bi, L.; Boulfrad, S.; Traversa, E. Y and Ni co-doped $BaZrO_3$ as a proton-conducting solid oxide fuel cell electrolyte exhibiting superior power performance. *J. Electrochem. Soc.* **2015**, *162*, F1498−F1503.

(19) Kreuer, K. D. Proton-conducting oxides. *Annu. Rev. Mater. Res.* **2003**, *33*, 333−359.
(20) Morejudo, S.; Zanón, R.; Escolástico, S.; Yuste-Tirados, I.; Malerød-Fjeld, H.; Vestre, P.; Coors, W.; Martínez, A.; Norby, T.; Serra, J.; et al. Direct conversion of methane to aromatics in a catalytic co-ionic membrane reactor. *Science* **2016**, *353*, 563−566.
(21) Ding, D.; Zhang, Y.; Wu, W.; Chen, D.; Liu, M.; He, T. A novel low-thermal-budget approach for the co-production of ethylene and hydrogen via the electrochemical non-oxidative deprotonation of ethane. *Energy Environ. Sci.* **2018**, *11*, 1710−1716.
(22) Zhu, C.; Hou, S.; Hu, X.; Lu, J.; Chen, F.; Xie, K. Electrochemical conversion of methane to ethylene in a solid oxide electrolyzer. *Nat. Commun.* **2019**, *10*, No. 1173.
(23) Zhang, X.; Ye, L.; Li, H.; Chen, F.; Xie, K. Electrochemical dehydrogenation of ethane to ethylene in a solid oxide electrolyzer. *ACS Catal.* **2020**, *10*, 3505−3513.
(24) Yang, L.; Wang, S.; Blinn, K.; Liu, M.; Liu, Z.; Cheng, Z.; Liu, M. Enhanced sulfur and coking tolerance of a mixed ion conductor for SOFCs: $BaZr_{0.1}Ce_{0.7}Y_{0.2-x}Yb_xO_{3-\delta}$. *Science* **2009**, *326*, 126−129.
(25) Wu, W.; Gaffney, A.; Ding, D. Electrochemical conversion of natural gas to value added chemicals. In*Direct Natural Gas Conversion to Value-Added Chemicals*; CRC Press, 2020; pp 1−24.
(26) Kreuer, K. Aspects of the formation and mobility of protonic charge carriers and the stability of perovskite-type oxides. *Solid State Ionics* **1999**, *125*, 285−302.
(27) Ding, H.; Fang, S.; Yang, Y.; Yang, Y.; Wu, W.; Tao, Z. High-performing and stable electricity generation by ceramic fuel cells operating in dry methane over 1000 hours. *J. Power Sources* **2018**, *401*, 322−328.
(28) Wu, W.; Zhang, Y.; Ding, D.; He, T. A high-performing direct carbon fuel cell with a 3D architectured anode operated below 600 C. *Adv. Mater.* **2018**, *30*, No. 1704745.
(29) Bian, W.; Wu, W.; Orme, C. J.; Ding, H.; Zhou, M.; Ding, D. Dual 3D ceramic textile electrodes: fast kinetics for carbon oxidation Reaction and oxygen reduction reaction in direct carbon fuel cells at reduced temperatures. *Adv. Funct. Mater.* **2020**, *30*, No. 1910096.
(30) Wu, W.; Ding, H.; Zhang, Y.; Ding, Y.; Katiyar, P.; Majumdar, P. K.; He, T.; Ding, D. 3D self-architectured Steam electrode enabled efficient and durable hydrogen production in a proton-conducting solid oxide electrolysis cell at temperatures lower than 600 °C. *Adv. Sci.* **2018**, *5*, No. 1800360.
(31) Bian, W.; Wu, W.; Gao, Y.; Gomez, J. Y.; Ding, H.; Tang, W.; Zhou, M.; Ding, D. Regulation of cathode mass and charge transfer by structural 3D engineering for protonic ceramic fuel cell at 400 °C. *Adv. Funct. Mater.* **2021**, No. 2102907.
(32) Ding, H.; Wu, W.; Jiang, C.; Ding, Y.; Bian, W.; Hu, B.; Singh, P.; Orme, C. J.; Wang, L.; Zhang, Y.; et al. Self-sustainable protonic ceramic electrochemical cells using a triple conducting electrode for hydrogen and power production. *Nat. Commun.* **2020**, *11*, No. 1907.
(33) Wang, L.-C.; Zhang, Y.; Xu, J.; Diao, W.; Karakalos, S.; Liu, B.; Song, X.; Wu, W.; He, T.; Ding, D.; et al. Non-oxidative dehydrogenation of ethane to ethylene over ZSM-5 zeolite supported iron catalysts. *Appl. Catal., B* **2019**, *256*, No. 117816.
(34) Thiruvenkataswamy, P.; Eljack, F. T.; Roy, N.; Mannan, M. S.; El-Halwagi, M. M. Safety and techno-economic analysis of ethylene technologies. *J. Loss Prev. Process Ind.* **2016**, *39*, 74−84.
(35) Sundaram, K. M.; Froment, G. F. Modeling of thermal cracking kinetics. 3. Radical mechanisms for the pyrolysis of simple paraffins, olefins, and their mixtures. *Ind. Eng. Chem. Fundam.* **1978**, *17*, 174−182.
(36) Kreuer, K.-D.; Paddison, S. J.; Spohr, E.; Schuster, M. Transport in proton conductors for fuel-cell applications: simulations, elementary reactions, and phenomenology. *Chem. Rev.* **2004**, *104*, 4637−4678.
(37) Hansen, M. H.; Nørskov, J. K.; Bligaard, T. First principles micro-kinetic model of catalytic non-oxidative dehydrogenation of ethane over close-packed metallic facets. *J. Catal.* **2019**, *374*, 161−170.
(38) Virnovskaia, A.; Morandi, S.; Rytter, E.; Ghiotti, G.; Olsbye, U. Characterization of Pt, Sn/Mg(Al)O catalysts for light alkane dehydrogenation by FT-IR spectroscopy and catalytic measurements. *J. Phys. Chem. C* **2007**, *111*, 14732−14742.

https://doi.org/10.1021/acscatal.1c03351
ACS Catal. 2021, 11, 12194−12202

Electrochemical Engineered, Highly Energy-Efficient Conversion of Ethane to Ethylene and Hydrogen below 550 °C in a Protonic Ceramic Electrochemical Cell

Wei Wu[1,‡,], Lu-Cun Wang[1,‡], Hongqiang Hu[1], Wenjuan Bian[1,2], Joshua Y. Gomez[1,2], Christopher J. Orme[1], Hanping Ding[1], Yanhao Dong[3], Ting He[1], Ju Li[3], and Dong Ding[1*]*

[1]Department of Energy & Environmental Science and Technology, Idaho National Laboratory, Idaho Falls, ID 83415, USA

[2]Department of Chemical & Materials Engineering, New Mexico State University, Las Cruces, NM 88003, USA

[3]Department of Nuclear Science and Engineering, Massachusetts Institute of Technology, Cambridge, MA, 02139, USA

[‡]These authors contributed equally.

*Corresponding Authors:

Wei Wu, E-mail: wei.wu@inl.gov

Dong Ding, E-mail: dong.ding@inl.gov

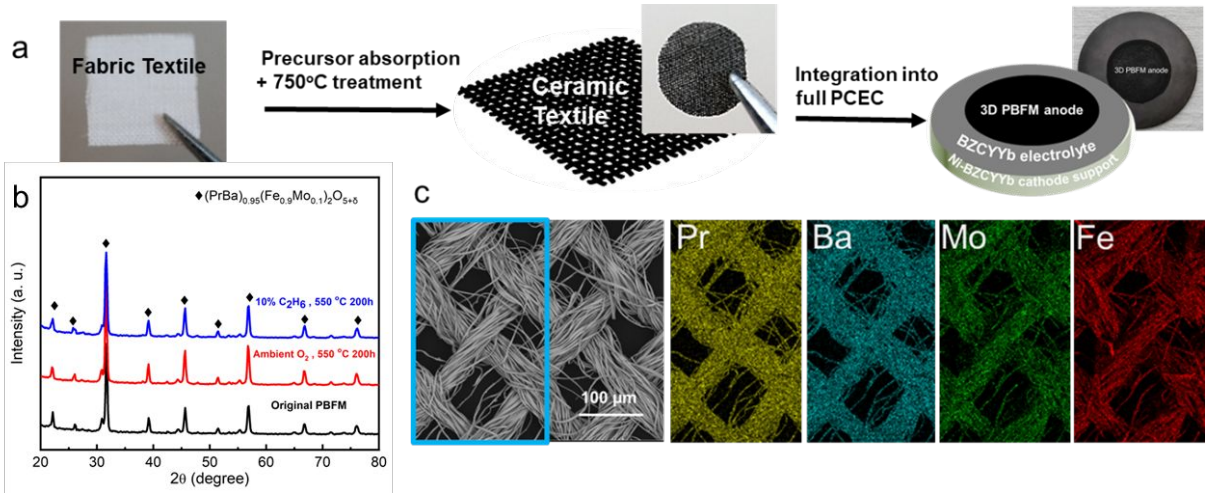

Figure S1. (a) Fabrication procedures of electrochemical cell with 3D anode. The 3D anode enables fast mass and charge transfer both in EEDC and SOEC mode. (b) XRD patterns of PBFM material under different atmospheres indicate good chemical stability. (c) EDS mapping results of PBFM textile show the well distribution of elements.

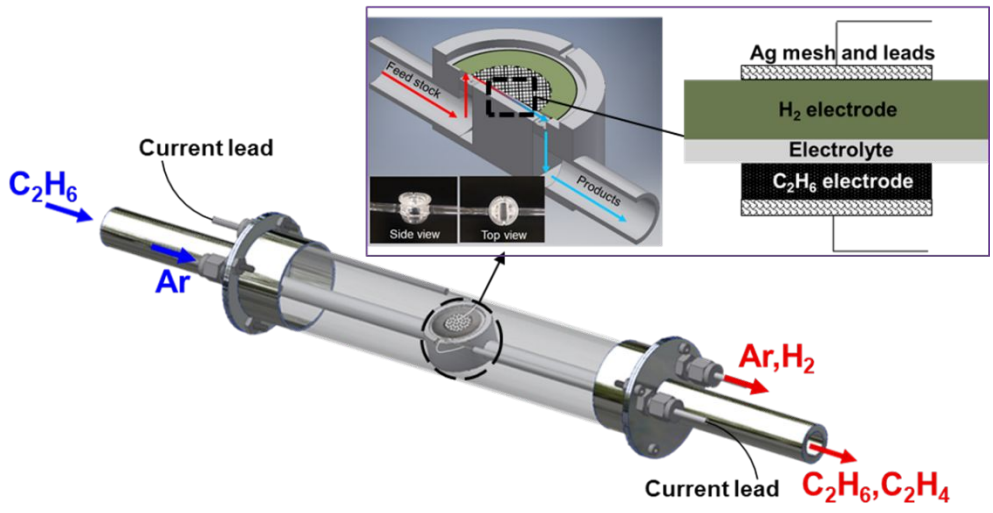

Figure S2. Schematic of the in-house built dual-zone reactor with quartz reacting bed inside. The horizontal design of gas flow can regulate the gas distribution in the reactor to reduce the risk of pressure accumulation, as well as ensuring a reasonable feedstock utilization.

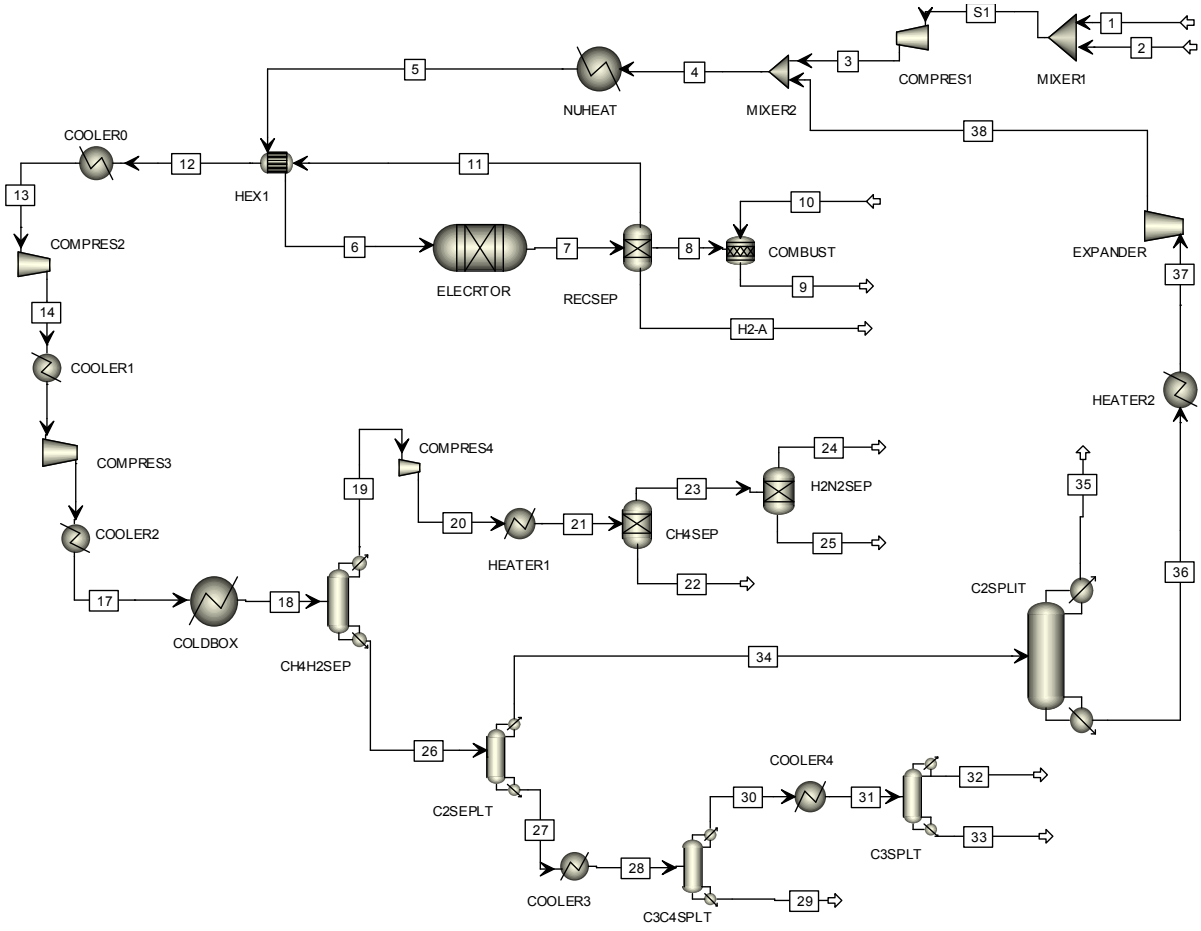

Figure S3. Detailed process flow diagram of an EEDC process for AspenPlus simulation.

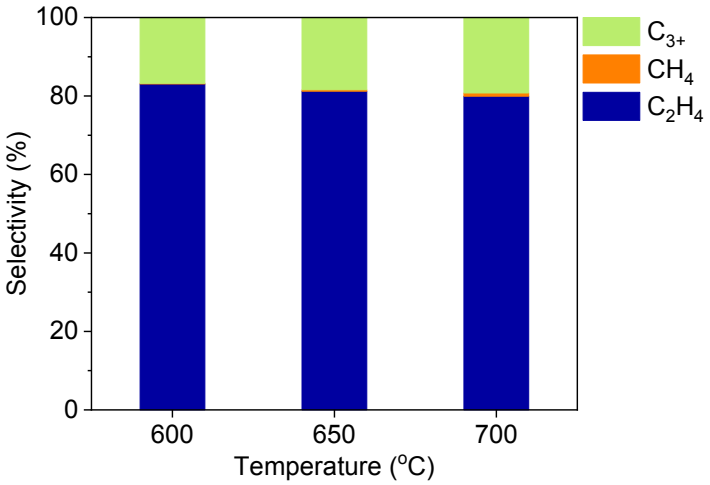

Figure S4. Selectivity of various hydrocarbon products in the EEDC process at different temperatures above 600 °C under OCV condition.

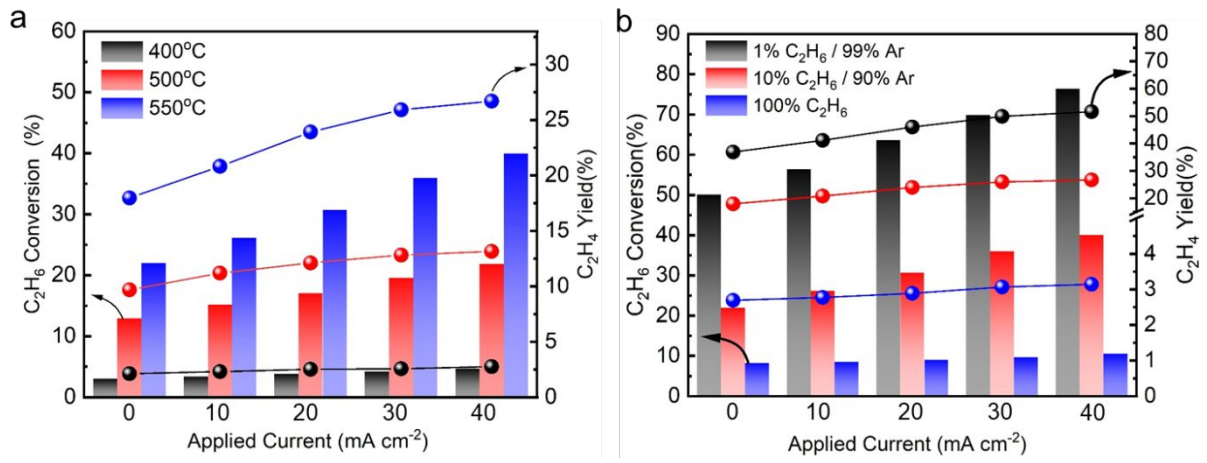

Figure S5. (a) C_2H_6 conversion and C_2H_4 yield at different operating temperatures with 10% C_2H_6 balanced with Ar as feedstock. (b) C_2H_6 conversion and C_2H_4 yield at 550 °C with different C_2H_6 feedstock concentration.

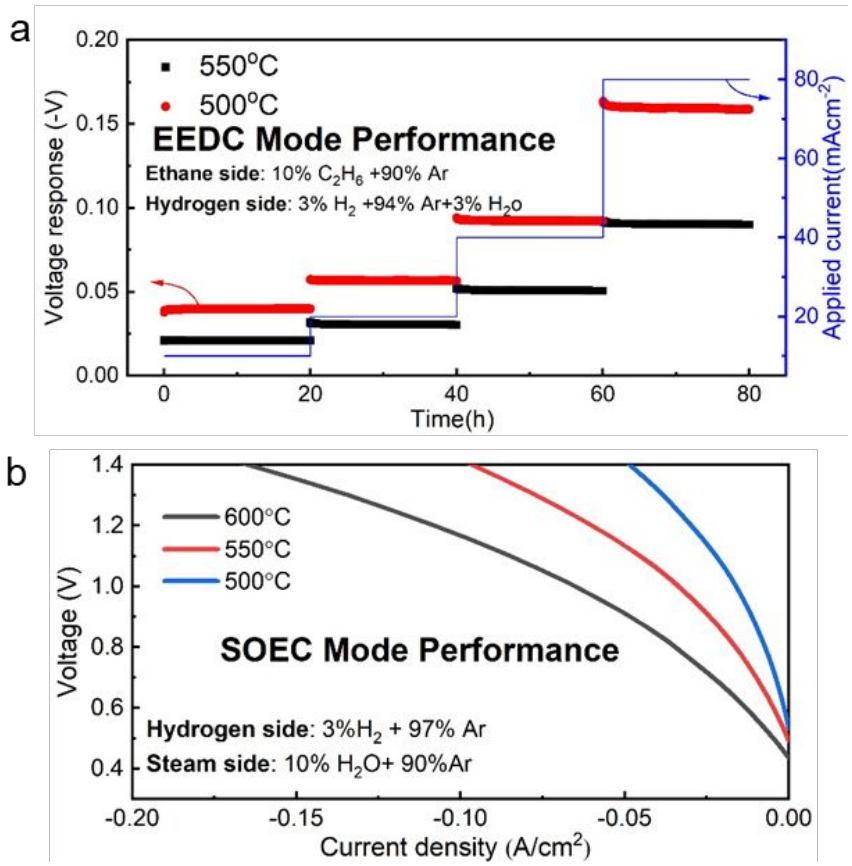

Figure S6. (a) The voltage responses during EEDC process. (b) SOEC performance of electrochemical cell with configuration of PBFM-BZCYYb steam electrode / BZCYYb / Ni-BZCYYb hydrogen electrode, at different operating temperatures. The hydrogen electrode atmosphere in SOEC is 3% H_2 balanced with argon, while that of cathode is 10% H_2O balanced with Ar. The electrolysis current density at 1.4 V increases with the operating temperature and reaches 165, 97 and 48 mA cm^{-2} at 600, 550 and 500 °C, respectively.

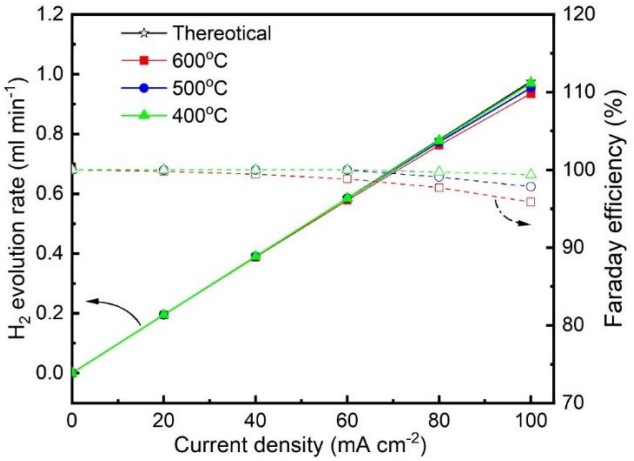

Figure S7. Results of Faraday efficiency measurement. In the EEDC process, ethane activation may be driven by both thermal and electrical energy, thus making it difficult to reliably deconvolute the contribution of electrochemical ethane conversion. Accordingly, the FE under EEDC operation is defined based on the hydrogen evolution reaction according to the following equation:

$$\eta = \frac{n_{H_2,\,actual}}{n_{H_2,\,theoretical}} = \frac{n_{H_2,\,actual}}{\mathrm{I} \times (\mathrm{n} \times \mathrm{F})^{-1}} \times 100\%$$

where η is the FE of the EEDC process, $n_{H_2,\,actual}$ is the actual and theoretical hydrogen production rate measured by GC analysis (mol·s^{-1}), $n_{H_2,\,theoretical}$ is the theoretical hydrogen production rate (mol·s^{-1}), I is the current (unit is A), n is 2, and F is Faraday's constant (96,485 A·s·mol^{-1}).

The decrease in FE at higher current densities may originate from two factors. One is the larger amount of heat generated from SOEC internal resistance than that required for water

decomposition at high current densities because of increasing operating voltage.[1] Another possible reason for the efficiency loss at higher current density may be the electronic or hole conduction, since the proton-conducting oxides are not unity at high voltage.[2] However, all the Faraday efficiencies at electrolysis voltages up to 1.8 V were close to the theoretical 100%, which indicated the current leakage through BZCYYb electrolyte could be negligible at 400°C.

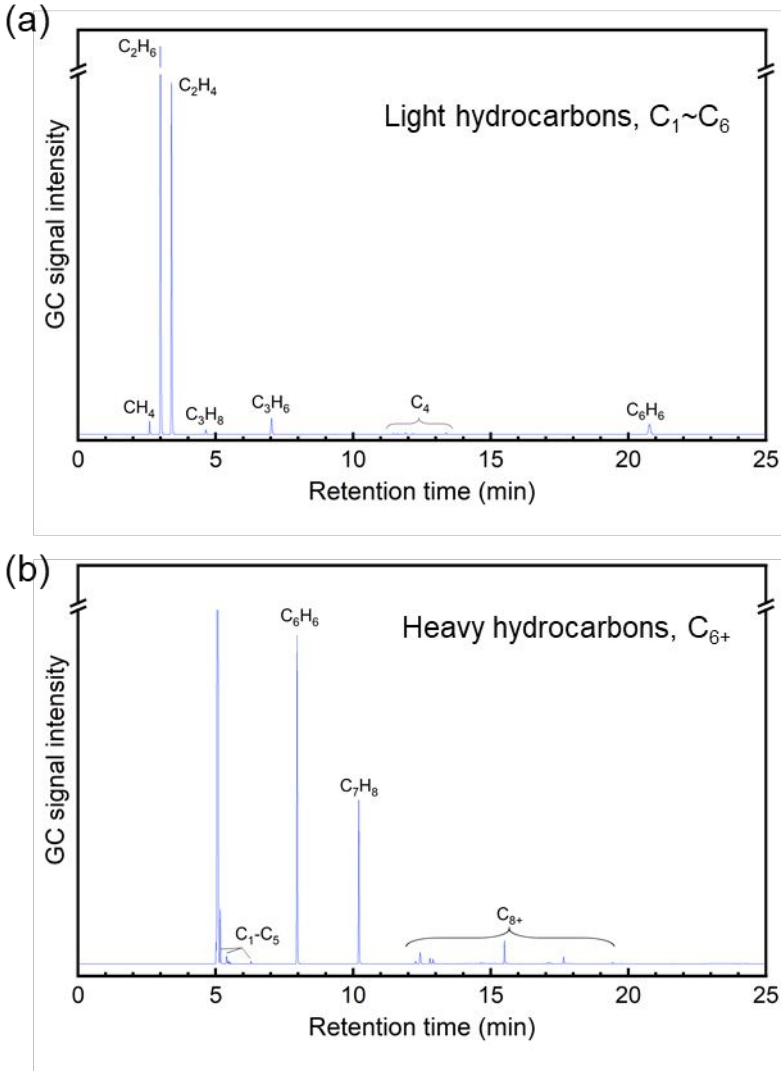

Figure S8. GC raw data showing the formation of higher (C_{3+}) hydrocarbon products in the EEDC process.

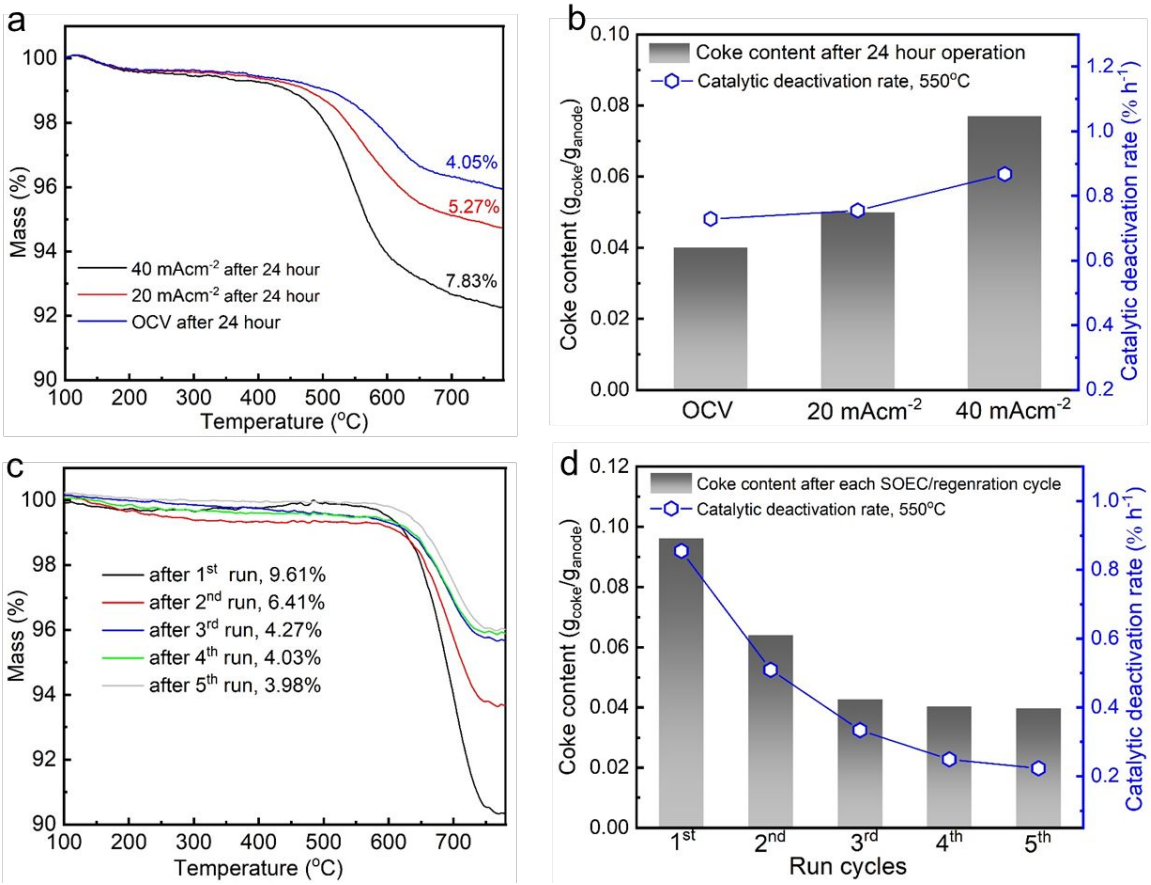

Figure S9. TGA results and calculated coke content. (a) TGA curves of anode under different applied current after 24 hours. (b) Coke content and relevant catalytic deactivation rate of EEDC at different applied current after 24 hours. (c) TGA curves of anode under different running cycles (1 cycle:30-h EEDC and 6-h SOEC). (d) The comparison of coke content and catalytic deactivation rate after each regeneration cycle.

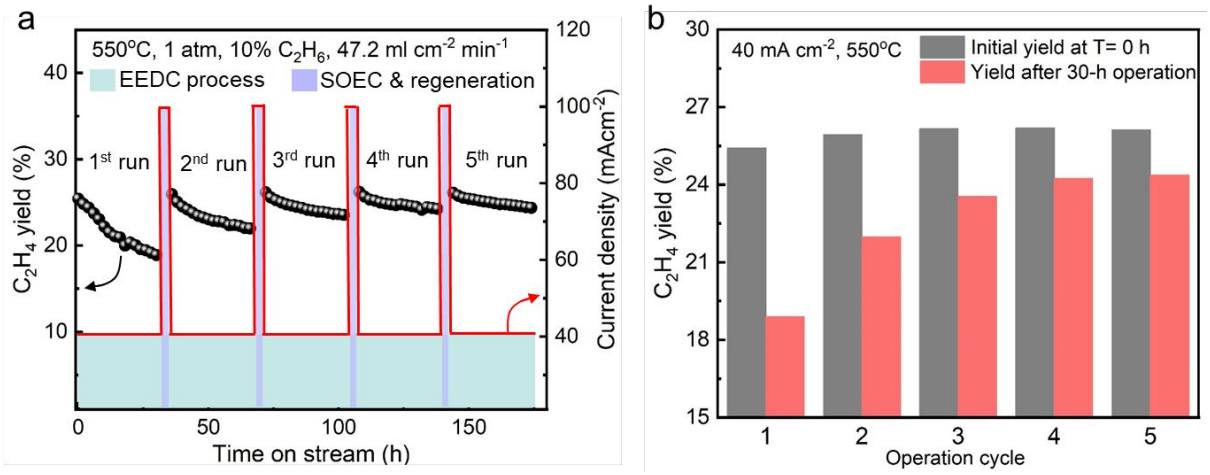

Figure S10. (a) C_2H_4 yield change during each operation cycle. After 30-h EEDC process, the system is operated under SOEC mode at 100 mA cm^{-2} for 6 hours to conduct steam electrolysis as well as to remove coke content. (b) Improvement both in initial C_2H_4 yield and catalytic durability. Anode reconstruction (i.e., fiber bridging effect) and catalyst particles redistribution happen during the operation, resulting in better catalyst utilization and lower cell ohmic loss.

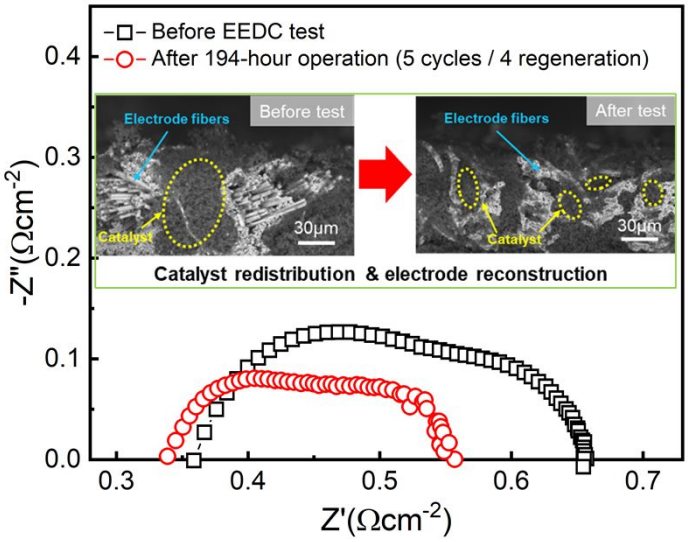

Figure S11. Cell resistance decreases due to 3D electrode reconstruction during EEDC/SOEC operation. Inserted SEM images showing the integrated anode morphology change before and after the test.

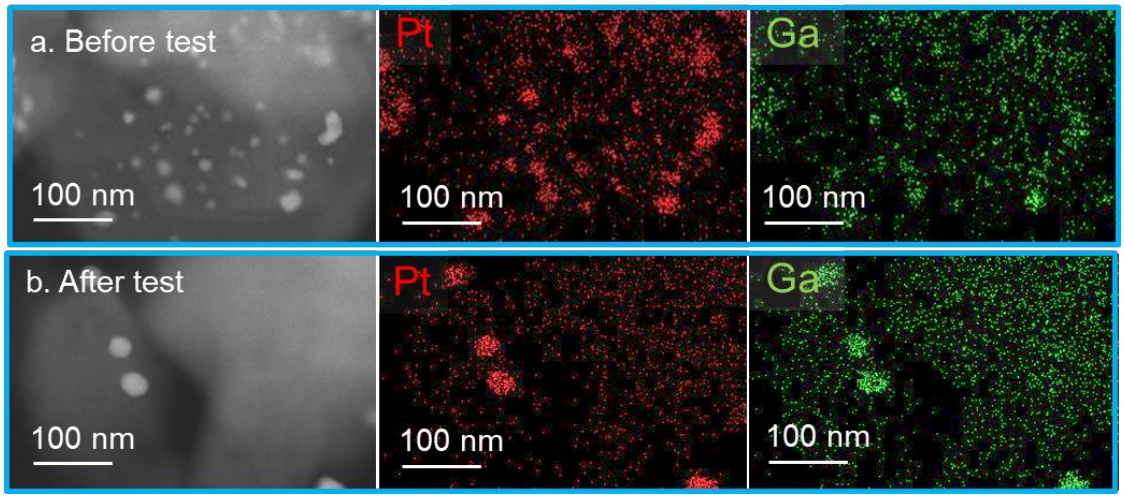

Figure S12. STEM image of PtGa/ZSM-5 catalyst. (a) Before EEDC process. (b) After EEDC process. Both Pt and Ga particles were redistributed on the ZSM-5 surface highly due to the SOEC operation, enhancing the catalyst anti-coking ability.

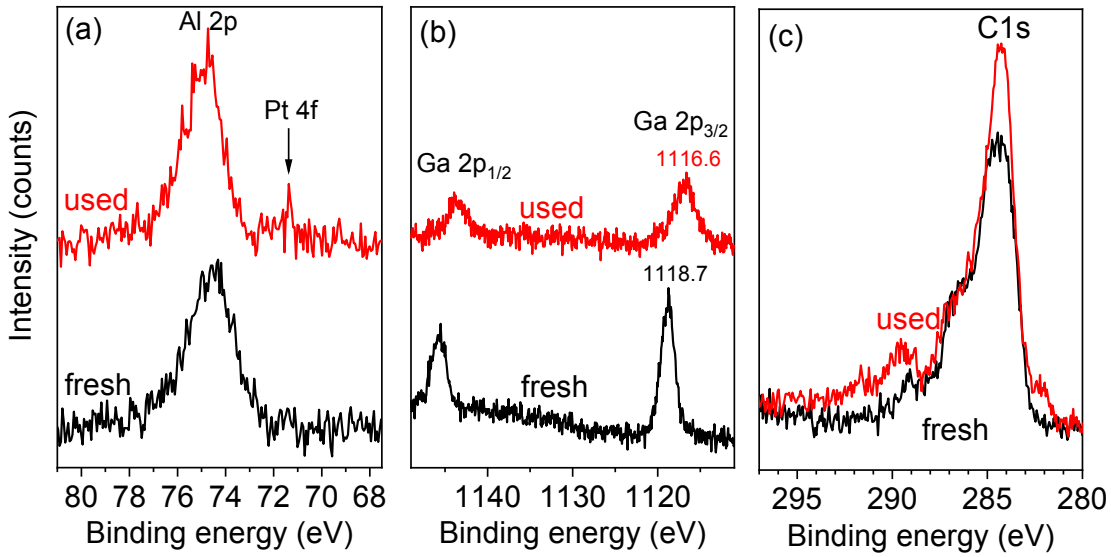

Figure S13. (a) Pt4f, (b) Ga2p, and (c) C1s XPS result of PtGa/ZSM-5 catalyst before and after reaction.

Table S1. Assumption for the AspenPlus simulation of the EEDC process

Unit	Design Assumption /Operating Conditions
EEDC	Operating at T=550 ℃, 15 psi. It was modeled by three separate units: a reactor using RSTOIC model; a separator for separating generated hydrogen and other products; and a reactor for decoking by burning the produced carbon.
Heat exchangers	Δp = 5 and 3 for hot and cold side, respectively. Min. ΔT=10 ℃. Shell-and -tube type.
Compressor	Turbine driven centrifugal compressor at multiple stages with intermediate cooling; Compressor-outlet temperatures are always less than 150 ˚C to avoid formation of polymers that plug equipment.
Refrigeration system/coldbox	This system further reduces the temperature of feeding stream for downstream cryogenic separation of various hydrocarbons in liquid condition to -150 ˚C and 145 psi. A multistage/cascade process to reach cryogenic temperatures and a coil-wound heat exchanger for heat transfer are applied in design.
Cryogenic Distillation column separation	Five columns, demethanizer, deethanizer, and depropanizer, C3 and C2 splitter, were modeled using RadFrac method. All products recovered from distillation are based on minimum 99% mass

	recovery except for ethylene/ethane and propane/propylene separation, which are 90%.
Membrane separation	Permeate purity, 99%

Table S2. Reactions and corresponding conversions inside the EEDC reactor at 40 $mA \cdot cm^{-2}$ assumed for AspenPlus simulation.

Reaction	Fractional conversion	Conversion of limiting reactant
$C_2H_6 = C_2H_4 + H_2$	0.363	Ethane
$2C_2H_6 = C_3H_8 + CH_4$	0.02	Ethane
$C_3H_8 = C_3H_6 + H_2$	0.8	Propane
$2C_2H_4 = C_4H_8$	0.23	Ethylene
$C_2H_6 + C_2H_4 = C_3H_6 + CH_4$	0.032	Ethylene
$CH_4 = C + 2H_2$ (Coke Formation)	0.07	Methane

Table S3. Process result summary of ethylene production from steam-ethane cracking and EEDC at applied current density of 40 mA cm^{-2}.

Parameter	**Unit**	**Steam Cracking**	**EEDC**
Annual Ethane Feed Rate	Metric Tonne/Yr	978,492	972,360
Annual Production Rate of Ethylene	Metric Tonne/Yr	830,132	636,125
Ethylene-Product Purity	%	99.90	99.90
Annual Production Rate of H_2	Metric Tonne/Yr	0 [a]	62,835
H_2 Product Purity	%	-	99.90
Ethane Single-Pass Conversion	%	**60**	**38**
Ethylene Single-Pass Yield	%	**52.4**	**26.7**
Process Yield of Ethylene	%	85	65
Operating temperature	˚C	850	550
Overall Specific-Energy Consumption w/o ethane feedstock	MMBTU/Metric Ton Ethylene	38	32
Overall Specific-Energy Consumption w/ ethane feedstock	MMBTU/Metric Ton Ethylene	90	100

Overall System Energy Efficiency	% (total energy input/energy output)	47	75
Operation Hours Per Year	Hour	8760	8760
Plant Lifetime	Year	20	20

[a] The off-gas generated from steam cracking process, including hydrogen, methane, acetylene, propylene, propane, and butadiene, are considered in the form of equivalent of natural gas for heating and are balanced in the final energy of fuel required.

Table S4. Specific energy input and output for the EEDC process.

	Specific Energy Requirement, MMBTU/metric ton C_2H_4				
	0 mA cm^{-2}	10 mA cm^{-2}	20 mA cm^{-2}	30 mA cm^{-2}	40 mA cm^{-2}
Electricity	29.27	27.7	26.3	23.67	23.28
Non-electricity	10.11	9.6	9.16	8.55	8.44
Ethane feed	84.22	75.56	70.47	68.58	68.39
Total input	123.60	112.86	105.93	100.80	100.11
Ethylene	45.25	45.25	45.25	45.25	45.25
Hydrogen	11.48	11.05	10.80	11.26	11.24
Other gases	25.25	22.09	20.16	19.02	18.87
Total output	81.98	78.39	76.21	75.53	75.37
Energy efficiency	66%	69%	71.9%	74.9%	75.3%

Table S5. Surface chemical composition of PtGa/ZSM-5 catalyst before and after reaction.

Sample	Atomic concentration (%)				
	Al	Si	C	Ga	Pt
fresh	1.6	26.5	6.7	0.7	n.d.[a]
used	1.3	25.9	9.1	0.4	n.d.

[a] not determined, due to below detection limit.

REFERENCE

1. Kreuer, K.-D.; Paddison, S. J.; Spohr, E.; Schuster, M., Transport in proton conductors for fuel-cell applications: simulations, elementary reactions, and phenomenology. *Chemical reviews* 2004, *104* (10), 4637-4678.

2. Morejudo, S. H.; Zanón, R.; Escolástico, S.; Yuste-Tirados, I.; Malerød-Fjeld, H.; Vestre, P. K.; Coors, W. G.; Martínez, A.; Norby, T.; Serra, J. M., Direct conversion of methane to aromatics in a catalytic co-ionic membrane reactor. *Science* 2016, *353* (6299), 563-566.